

© 2022 IEEE. Personal use of this material is permitted. Permission from IEEE must be obtained for all other uses, including reprinting/republishing this material for advertising or promotional purposes, collecting new collected works for resale or redistribution to servers or lists, or reuse of any copyrighted component of this work in other works. This work has been submitted to the IEEE for possible publication. Copyright may be transferred without notice, after which this version may no longer be accessible.

arXiv:2209.14823v1 [cs.LG] 29 Sep 2022

Physical Human-Robot Interaction Control of an Upper Limb Exoskeleton with a Decentralized Neuro-Adaptive Control Scheme

Mahdi Hejrati , Jouni Mattila , *Member, IEEE*

Abstract—In the concept of physical human-robot interaction (pHRI), the most important criterion is the safety of a human operator interacting with a high degrees of freedom (DoF) robot. Therefore, a robust control scheme is of high demand to establish safe pHRI and stabilize nonlinear, high DoF systems. In this paper, an adaptive decentralized control strategy is designed to accomplish mentioned objectives. To do so, human upper limb model and exoskeleton model are decentralized and augmented at the subsystem level to be able to design a decentralized control action. Moreover, human exogenous force (HEF) that can resist exoskeleton motion is estimated using radial basic function neural networks (RBFNNs). Estimating both human upper limb and robot rigid body parameters along with HEF estimation makes the controller adaptable to different operators, ensuring their physical safety. The *barrier Lyapunov function* (BLF), on the other hand, is employed to guarantee that the robot will work in a safe workspace while ensuring stability by adjusting the control law. Additionally, unknown actuator uncertainty and constraints are considered in this study to ensure a smooth and safe pHRI. Then, the asymptotic stability of the whole system is established by means of the *virtual stability* concept and *virtual power flows* (VPFs). Numerical and experimental results are provided and compared to PD controller to demonstrate the excellent performance of the proposed controller. As a result, the proposed controller accomplished all the control objectives with nearly zero error and low computed torque, ensuring physical safety in pHRI.

Index Terms—Adaptive decentralized control, Input and state constraints, Physical human-robot interactions, Wearable robots,

I. INTRODUCTION

PHYSICAL human-robot interaction (pHRI) combines human and robotic capabilities through physical interaction to carry out an assigned task. The typical application modes of such an interaction are assistance, cooperation, and teleoperation. Exoskeletons are wearable robots that can work in both assistance and teleoperation modes. In assistance mode, pHRI can be either for a short time, such as doing daily tasks, or for a long time, such as a power extender [1]. In teleoperation mode, exoskeletons are utilized as master robots that are worn by the operator, sending commands to

a slave robot. Therefore, pHRI lasts until the task on the slave side is executed [2]. These applications all require close, safe, and dependable physical interactions between human and robot within a common workspace [3]. The research goal in safe pHRI has three categories: interaction safety assessment, interaction safety through design, and interaction safety through planning and control [4]. In this paper, pHRI safety through control is studied, and a decentralized control scheme is designed to ensure safety and accomplish control objectives.

Generally, exoskeletons work actively or passively. The goal of passive exoskeletons is to track the desired trajectory while carrying a human limb. An active exoskeleton helps humans accomplish a task while compensating for part of the required force [5]. Both approaches have been widely examined in the literature [6]. In [7], an iterative estimator-based backstepping control has been utilized to study an upper limb exoskeleton in passive mode. In [8], dynamic uncertainty has been handled utilizing the time delay estimation (TDE) method, and an adaptive backstepping control method has been employed to achieve control goals. RBFNNs along with an adaptive backstepping sliding mode control (SMC) method have been utilized in [9] to address uncertainty and achieve control objectives. The compliant control of an upper limb exoskeleton based on SMC has been investigated in [10]. Moreover, in [11], integral second-order SMC has been exploited for the control problem of upper limb exoskeletons. Although the above-mentioned control schemes have shown good performance, they are not perfect choices for ensuring safety in pHRI with high DoF systems. For example, backstepping can result in an explosion of complexity, even for a simple system [12]. In this paper, to ensure safe pHRI of high DoF robots, such as the 7 DoF upper limb exoskeleton in this study, a decentralized control scheme is designed. The employed controller, named virtual decomposition control (VDC), is perfect for our objective for a number of reasons: *i*) it breaks down the entire complex system into subsystems and designs controller and analysis stability at the subsystem level, *ii*) changes in the dynamics or subsystem control signals do not affect the control equations of the rest of the system, *iii*) it divides the model into rigid body and actuator dynamics part, enabling us to examine unmodeled dynamics separately in both parts. In subsection A, more detail is provided about the control method.

There are a number of aspects that must be considered in the control design to guarantee interaction safety through control

The TITAN (Teaching human-like abilities to heavy mobile manipulators through multisensory presence) project is funded by the Technology Industries of Finland Centennial Foundation and the Jane and Aatos Erkko Foundation Future Makers programme. 2020-2023.

M. Hejrati, corresponding author, is with the Department of Engineering and Natural Science, Tampere University, 7320 Tampere, Finland (e-mail: mahdi.hejrati@tuni.fi).

J. Mattila is with the Department of Engineering and Natural Science, Tampere University, 7320 Tampere, Finland (e-mail: Jouni.Mattila@tuni.fi).

during pHRI. The first issue is actuator input constraints, for instance, backlash, saturation or dead zones. Actuator constraints widely exist in robotic systems and can destroy control performance and result in instability and unsafe pHRI [13]. One well-known approach to address these constraints is RBFNNs. In [14], RBFNNs have been employed to estimate dead zones. In [15], RBFNNs along with an auxiliary term has been introduced to handle input saturation. However, in these works, only one constraint has been considered, whereas in real-world robotic systems, two or more constraints, e.g., input saturation and dead zones, can exist. One aim of this work is to consider combined input constraints, incorporating input saturation and dead zones.

The second factor is state constraints. Although the mechanical range of exoskeletons is achievable for human operators, some postures can cause harm to operators due to fast robot movement, applied high torque from robot to operator, or high tracking error. To take this constraint into account, the barrier Lyapunov function (BLF) with tangent, cosecant, and logarithm functions is utilized in the literature [16]–[18]. In this work, for the first time in the context of the VDC approach, the logarithmic BLF is utilized to modify the control law to handle state constraints.

The third factor that can affect the safety of pHRI is the accuracy of the represented dynamics of the human limb and robot. Due to the existence of unmodeled dynamics in the robot model, operating at high frequency can excite those unmodeled dynamics and result in instability and unsafe pHRI. Numerous works have been performed to address unmodeled dynamics in robotic systems [19], [20]. In addition to robot dynamics, human limb dynamics must be considered in the pHRI model. In [21], the impact of human dynamics on pHRI has been investigated, and its importance has been shown. To consider human upper limb dynamics in interaction with exoskeletons, number of challenges must be overcome, e.g., estimating human exogenous forces and deriving inertia, damping, and stiffness matrices for a second order dynamic model. Different methods have been proposed to estimate human exogenous forces. In [22], [23], exogenous force has been estimated using a fast parameter adaptation function. In [24], human exogenous force has been expressed in linear-in-parameter form, and the unknown constant part was estimated by a projection function. In the mentioned research, different approaches has been proposed to estimate human exogenous forces and unmodeled dynamics. In this work, RBFNNs are exploited to both estimate human exogenous forces and address unmodeled dynamics. In recent decades, many works have been performed to derive human arm matrices. In [25], a human arm impedance model has been estimated by an adaptive control approach and considered in the control of an upper limb exoskeleton. In [26], multilayer perceptron (MLP) networks has been utilized to extract arm impedance model matrices. However, in the above-mentioned works, the impedance model of human arm has been studied, while integrating human arm dynamics and robot dynamics through a decentralized control scheme requires that the inertia, damping, and stiffness matrices of human arm must be defined in a joint space. In this study, human arm model is decentralized

and augmented to a robot model that enables us to estimate both inertial parameters of the arm and HEF.

A. Virtual Decomposition Control

Virtual decomposition control (VDC) [27] keeps the overall robotic system asymptotically stable by using subsystem dynamics (link connections and joints). The use of a scalar term called the virtual power flow (VPF), which is defined as the inner product of the velocity error and the force error in a common frame, is one element of this method. The VPF is introduced at each virtual cutting point where a virtual "disconnection" is placed. The VPF serves as a distinctive definition of the dynamic interaction between subsystems and is essential in defining the virtual stability of each subsystem. As a result, this method is specifically designed for controlling complex systems, with a number of significant state-of-the-art control performance improvements with robotic systems [28]–[31]. One benefit of employing the VDC method is that any changes to a subsystem's dynamics only impact the local control equations specific to that subsystem, leaving the control equations for the rest of the system unaffected [27].

Despite all the above-mentioned advantages of VDC, it uses a projection function for parameter estimation, which requires $13n$ adaptation gain and $26n$ upper and lower parameter bounds, with n being the number of rigid bodies. In cases of high DoF systems, providing such a long list of parameters is arduous. In [32], the VDC approach is utilized to control a 7 DoF exoskeleton with a projection function for parameter estimation. To remove the projection function, in [33], we proposed a novel VDC scheme that exploits the natural adaptation law (NAL) function to estimate unknown parameters. The NAL function only requires one adaptation gain for the entire system and removes upper and lower bounds, while ensuring a physical consistency condition. Moreover, the dynamics of the rigid body represented in the original VDC context is reformulated to make it compatible with the NAL, resulting in a compact formulation [33]. Therefore, taking advantage of this novel VDC scheme enables us to break down the entire complex pHRI to compact subsystems and design a decentralized adaptive controller with only one adaptation gain for the entire system, while ensuring stability of the entire system. Additionally, in [32], only joint control is studied, whereas in this paper we considered a human-robot model with unknown input and state constraints.

B. Aims and Contributions

The aim of this paper is to employ VDC as a decentralized control scheme to control pHRI in the presence of unknown unmodeled dynamics and input constraints. To have a safe pHRI, state constraints are considered and handled by exploiting BLF. Moreover, to have a much more accurate pHRI model and high safety, both human exogenous forces and human arm characteristics, i.e., mass, damping, and stiffness matrices, which are defined at the subsystem level, are estimated in this paper. RBFNNs are also exploited to address unknown combined input constraints and unmodeled dynamics. It is worth mentioning that each of these contributions is being

made for the first time in the context of the VDC approach. The contributions of this paper can be expressed as follows.

- An augmented human-robot model is derived and utilized for VDC control design.
- RBFNNs are employed to estimate human exogenous force and address unmodeled dynamics and input constraints. The input constraint in this study is a combination of input saturation and dead zones.
- BLF is exploited to apply state constraints to the system. This ensures the physical safety of pHRI as well as asymptotic stability.

The rest of the paper is organized as follows. Section II expresses the fundamental mathematics of the VDC approach along with the essential lemmas and definitions utilized in this paper. Section III describes the procedure of decentralization and augmentation of human upper limb dynamics with robot dynamics at the subsystem level. Control design and stability analysis are performed in Section IV. Experimental and numerical results are provided in Section V, and the validity of the stability and control results are proven. Finally, Section VI concludes this study.

II. MATHEMATICAL PRELIMINARIES

A. VDC Foundations

Consider $\{A\}$ as a frame that is attached to a rigid body. Then, the 6D linear/angular velocity vector ${}^A\mathcal{V} \in \mathbb{R}^6$ and force/moment vector ${}^A\mathcal{F} \in \mathbb{R}^6$ can be expressed as follows [27]:

$${}^A\mathcal{V} = [{}^A v, {}^A \omega]^T, \quad {}^A\mathcal{F} = [{}^A f, {}^A m]^T$$

where ${}^A v \in \mathbb{R}^3$ and ${}^A \omega \in \mathbb{R}^3$ are the linear and angular velocities of frame $\{A\}$, and ${}^A f \in \mathbb{R}^3$ and ${}^A m \in \mathbb{R}^3$ are the force and moment expressed in frame $\{A\}$, respectively. The transformation matrix that transforms force/moment vectors and velocity vectors between frames $\{A\}$ and $\{B\}$, where $\{B\}$ is another frame attached to the rigid body, is [27],

$${}^A U_B = \begin{bmatrix} {}^A R_B & \mathbf{0}_{3 \times 3} \\ ({}^A r_{AB \times}) {}^A R_B & {}^A R_B \end{bmatrix} \quad (1)$$

where ${}^A R_B \in \mathbb{R}^{3 \times 3}$ is a rotation matrix between frame $\{A\}$ and $\{B\}$, and ${}^A r_{AB \times}$ is a skew-symmetric matrix operator defined as,

$${}^A r_{AB \times} = \begin{bmatrix} 0 & -r_z & r_y \\ r_z & 0 & -r_x \\ -r_y & r_x & 0 \end{bmatrix} \quad (2)$$

where ${}^A r_{AB} = [r_x, r_y, r_z]^T$ denotes a vector from the origin of frame $\{A\}$ to the origin of frame $\{B\}$, expressed in $\{A\}$. Based on the ${}^A U_B$, the force/moment and velocity vectors can be transformed between frames as [27],

$${}^B \mathcal{V} = {}^A U_B^T {}^A \mathcal{V}, \quad {}^A \mathcal{F} = {}^A U_B {}^B \mathcal{F}. \quad (3)$$

Then, the dynamic equation of the free rigid body expressed in frame $\{A\}$ can be derived as follows [33]:

$$M_A \frac{d}{dt} ({}^A \mathcal{V}) + C_A ({}^A \mathcal{V}) + G_A = {}^A \mathcal{F}^* \quad (4)$$

where $M_A \in \mathbb{R}^{6 \times 6}$ is the mass matrix, $C_A \in \mathbb{R}^{6 \times 6}$ is the centrifugal and Coriolis matrix, $G_A \in \mathbb{R}^6$ is the gravity vector, and ${}^A \mathcal{F}^* \in \mathbb{R}^6$ is the net force/moment vector applied to the rigid body. A detailed formulation of the matrices is provided in [33].

In the VDC approach, the required velocity is utilized instead of the desired velocity. The required velocity encompasses the desired velocity along with one or two error terms related to the position or force error in the position or force control mode, respectively. The required joint velocity can be defined as,

$$\dot{q}_r = \dot{q}_d + \lambda(q_d - q) \quad (5)$$

where λ is a positive constant, q is the joint angle, and \dot{q}_d and q_d are desired joint angular velocity and desired angle, respectively. The required linear/angular velocity vector ${}^A \mathcal{V}_r \in \mathbb{R}^6$ defined in frame $\{A\}$ can be derived by utilizing (5) and the kinematic relations from the base to the end-effector. Then, the required net force/moment vector can be defined as,

$${}^A \mathcal{F}_r^* = M_A \frac{d}{dt} ({}^A \mathcal{V}_r) + C_A ({}^A \mathcal{V}_r) + G_A + {}^A \mathcal{F}_c \quad (6)$$

where ${}^A \mathcal{F}_c$ is the VDC control term. In the original VDC [27], ${}^A \mathcal{F}_c$ is only a proportional velocity term that engenders control performance problems in experiments and is difficult to tune the corresponding gain parameter. In this study, a much more sophisticated term is proposed to accomplish control objectives. Moreover, an integral velocity term is added to ${}^A \mathcal{F}_c$, which removes control performance problems.

The VDC approach breaks down the entire complex system into subsystems at each *virtual cutting point* (VCP) and ensures the stability of the entire system by means of the *virtual stability* concept. VPFs will be defined and used to characterize the dynamic interactions among subsystems. The introduction of this terminology is an important step leading to the definition of virtual stability.

Definition 1. [27] A non-negative accompanying function $\nu(t) \in \mathbb{R}$ is a piecewise, differentiable function possessing two properties: $\nu(t) \geq 0$ for $t > 0$, and $\dot{\nu}(t)$ exists almost everywhere.

Definition 2. [27] With respect to frame $\{A\}$, the VPF is defined as the inner product of the linear/angular velocity vector error and the force/moment vector error, that is,

$$p_A = ({}^A V_r - {}^A V)^T ({}^A F_r - {}^A F) \quad (7)$$

where ${}^A \mathcal{V}_r \in \mathbb{R}^6$ and ${}^A \mathcal{F}_r \in \mathbb{R}^6$ represent the required vectors of ${}^A \mathcal{V} \in \mathbb{R}^6$ and ${}^A \mathcal{F} \in \mathbb{R}^6$, respectively.

Definition 3. [27] A subsystem that is virtually decomposed from a complex robot is said to be virtually stable with its affiliated vector $\mathcal{X}(t)$ being a virtual function and its affiliated vector $y(t)$ being a virtual function if and only if there exists a non-negative accompanying function

$$\nu(t) \geq \frac{1}{2} \mathcal{X}(t)^T P \mathcal{X}(t) \quad (8)$$

such that,

$$\dot{\nu}(t) \leq -y(t)^T Q y(t) + p_A - p_C \quad (9)$$

holds, subject to,

$$\int_0^\infty s(t)dt \geq -\gamma_s \quad (10)$$

with $0 \leq \gamma_s < \infty$, where P and Q are two block-diagonal positive-definite matrices, and p_A and p_C denote the sum of VPFs in the sense of Definition 2 at frames $\{A\}$ (placed at driven VCPs) and $\{C\}$ (placed at driving VCPs).

Theorem 1. [27] Consider a complex robot that is virtually decomposed into subsystems. If all the decomposed subsystems are virtually stable in the sense of Definition 1, then the entire system is stable.

Theorem 1 is the most important theorem in the VDC context. It establishes the equivalence between the virtual stability of every subsystem and the stability of the entire complex robot. Consequently, it allows us to concentrate on ensuring the virtual stability of every subsystem in lieu of the stability of the entire complex robot.

B. Lemmas and Definitions

In this part, all the lemmas and assumptions that are utilized in this paper are presented.

Assumption 1. For an external disturbance $F_d(t)$ and for human exogenous force $\tau_h(t)$, the following conditions are satisfied:

$$|F_d(t)| \leq \delta_1, \quad |\tau_h(t)| \leq \delta_2$$

with $\delta_1 \geq 0$, $\delta_2 \geq 0$ being unknown constants.

Assumption 2. For the unknown robot model uncertainties Δ_{Fr} and $\Delta_{\tau r}$, along with human arm unmodeled dynamics Δ_{Fh} and $\Delta_{\tau h}$, we have,

$$|\Delta_{Fr}| \leq \delta_3, \quad |\Delta_{\tau r}| \leq \delta_4, \quad |\Delta_{Fh}| \leq \delta_5, \quad |\Delta_{\tau h}| \leq \delta_6$$

where $\delta_3, \delta_4, \delta_5, \delta_6$ are positive unknown constants.

Lemma 1. [34] RBFNNs can be utilized to estimate an unknown continuous function $Z(\chi) : \mathbb{R}^m \rightarrow \mathbb{R}$ with the approximation of,

$$Z(\chi) = \hat{W}^T \Psi(\chi) + \hat{\varepsilon}$$

where $\chi = [\chi_1, \chi_2, \dots, \chi_m]^T \in \mathbb{R}^m$ is the input vector of the neural networks, \hat{W} is the weight vector of the neural networks, $\Psi(\chi)$ is the basis function of the RBFNNs, and $\hat{\varepsilon}$ is the approximation error. The optimal weight vector W^* can be expressed by,

$$W^* = \arg \min_{\hat{W} \in \Xi_N} \left\{ \sup_{\chi \in \Xi_T} |\hat{Z}(\chi|\hat{W}) - Z(\chi)| \right\}$$

where $\Xi_N = \{\hat{W} | \|\hat{W}\| \leq \kappa\}$ is a valid set of vectors with κ being a design value, Ξ_T is an allowable set of the state vectors, and $\hat{Z}(\chi|\hat{W}) = \hat{W}^T \Psi(\chi)$.

Lemma 2. [35] For any positive constant k_b , let $\mathfrak{Z} := \{\mathfrak{z} \in \mathbb{R} : -k_b < \mathfrak{z} < k_b\} \subset \mathbb{R}$ and $\mathcal{N} := \mathbb{R}^l \times \mathfrak{Z} \subset \mathbb{R}^{l+1}$ be open sets. Consider the system,

$$\dot{\eta} = \hat{h}(t, \eta)$$

where $\eta := [\omega, \mathfrak{z}]^T \in \mathcal{N}$, and $\hat{h} : \mathbb{R}_+ \times \mathcal{N} \rightarrow \mathbb{R}^{l+1}$ is piecewise continuous in t and locally Lipschitz in \mathfrak{z} , uniformly in t , on $\mathbb{R}_+ \times \mathcal{N}$. Suppose that there exist functions $\mathfrak{U} : \mathbb{R}^l \rightarrow \mathbb{R}_+$ and

$\mathfrak{V} : \mathfrak{Z} \rightarrow \mathbb{R}_+$, continuously differentiable and positive definite in their respective domains, such that,

$$\mathfrak{V}(\mathfrak{z}) \rightarrow \infty \quad \text{as } \mathfrak{z} \rightarrow -k_b \quad \text{or } \mathfrak{z} \rightarrow k_b$$

$$\delta_7(\|\omega\|) \leq \mathfrak{U}(\omega) \leq \delta_8(\|\omega\|)$$

where δ_7 and δ_8 are class \mathcal{K}_∞ functions. Let $V(\eta) := \mathfrak{V}(\mathfrak{z}) + \mathfrak{U}(\omega)$, and $\mathfrak{z}(0)$ belong to the set $\mathfrak{z} \in (-k_b, k_b)$. If the following inequality holds:

$$\dot{V} = \frac{\partial V}{\partial \eta} \dot{\eta} \leq 0$$

then $\mathfrak{z}(t)$ remains in the open set $\mathfrak{z} \in (-k_b, k_b) \forall t \in [0, \infty)$.

Remark 1. In Lemma 2, the state space is split into \mathfrak{z} and ω , where \mathfrak{z} is the state to be constrained, and ω is the free state. The constrained state \mathfrak{z} requires the barrier function \mathfrak{V} to prevent it from reaching the limits $-k_b$ and k_b , while the free states may involve quadratic functions.

Lemma 3. [36] [33] For any inertial parameter vector of a rigid body ϕ_A there is a one-to-one linear map $f : \mathbb{R}^{10} \rightarrow S(4)$, such that,

$$f(\phi_A) = \mathcal{L}_A = \begin{bmatrix} 0.5tr(\bar{I}_A) \cdot \mathbf{1} - \bar{I}_A & h_A \\ h_A^T & m_A \end{bmatrix}$$

$$f^{-1}(\phi_A) = \phi_A(m_A, h_A, tr(\Sigma_A) \cdot \mathbf{1} - \Sigma_A)$$

where m_A, h_A , and \bar{I}_A are the mass, first mass moment, and rotational inertia matrix, respectively. $\mathcal{L}_A \in S(4)$ is pseudo inertia matrix and $\Sigma_A = 0.5tr(\bar{I}_A) - \bar{I}_A$.

Lemma 4. [37] If Π is considered a signal exerted to the system and π be the designed control signal, the issue of input saturation along with input dead zones can be transformed into an equivalent input saturation form as,

$$\begin{aligned} \Pi &= \mathfrak{P}(\text{sat}(\mathfrak{P}^+(\pi))) \\ &= \begin{cases} k_r(k_M - m_r) & \text{if } \pi \geq k_r(k_M - m_r) \\ \pi & \text{if } k_l(k_m - m_l) < \pi < k_r(k_M - m_r) \\ k_l(k_m - m_l) & \text{if } \pi \leq k_l(k_m - m_l) \end{cases} \end{aligned}$$

where $k_M > 0$ and $k_m < 0$ are unknown upper and lower saturation levels, $m_r > 0$ and $m_l < 0$ are the unknown dead zones ranges, and $k_l > 0$ and $k_r < 0$ are the unknown slope parameters. Also, \mathfrak{P}^+ is the right inverse of \mathfrak{P} which satisfies $\mathfrak{P} \cdot \mathfrak{P}^+ = I$, and $\text{sat}(a)$ is the saturation function, defined as,

$$\text{sat}(a) = \begin{cases} a_{max} & \text{if } a \geq a_{max} \\ a & \text{if } a_{min} \leq a \leq a_{max} \\ a_{min} & \text{if } a \leq a_{min} \end{cases}$$

where a_{min} and a_{max} are the lower and upper limits of a , respectively.

III. DECENTRALIZATION AND AUGMENTATION OF THE HUMAN-ROBOT MODEL

In this section, the decentralized model of pHRI is derived. Robot dynamics is merged with human arm dynamics through the VDC context, which enables us to design a decentralized controller to accomplish safe interaction.

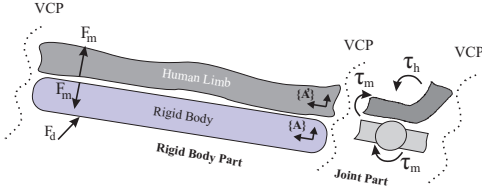


Fig. 1. Human-robot interaction model

A. Rigid Body Part

Inspired by (4) and Fig. 1, the dynamics of a rigid body in free space in the presence of unmodeled dynamics expressed in frame $\{A\}$ can be explained as,

$$M_A \frac{d}{dt}({}^A \mathcal{V}) + C_A({}^A \mathcal{V}) + G_A + \Delta_{Fr} = \mathcal{B}_1({}^A \mathcal{F}^*) - F_d - F_m \quad (11)$$

where $\mathcal{B}_1(\cdot)$ is the internal combined input constraint in the sense of Lemma 4, F_d is the unknown disturbance, F_m is the interaction force between human arm link and robot rigid body, and Δ_{Fr} is the unknown unmodeled dynamics of the rigid body. On the other hand, utilizing the VCP concept, human arm's link dynamics expressed in frame $\{A'\}$, can be written as,

$${}^h M_{A'} \frac{d}{dt}({}^{A'} \mathcal{V}_h) + {}^h C_{A'}({}^{A'} \mathcal{V}_h) + {}^h G_{A'} + \Delta_{Fh} = F_m \quad (12)$$

where Δ_{Fh} is the unknown unmodeled dynamics of human arm link, and ${}^h(\cdot)$ and $(\cdot)_h$ stands for human. We suppose that $\{A'\}$ and $\{A\}$ overlap. Therefore, by substituting (12) in (11) and using $\mathcal{B}_1({}^A \mathcal{F}^*) = {}^A \mathcal{F}^* - {}^A \Delta \mathcal{F}^*$ along with defining $\Delta_D = \Delta_{Fh} + \Delta_{Fr} + {}^A \Delta \mathcal{F}^*$, we obtain,

$$\mathcal{M}_A \frac{d}{dt}({}^A \mathcal{V}) + \mathcal{C}_A({}^A \mathcal{V}) + \mathcal{G}_A = {}^A \mathcal{F}^* - F_d - \Delta_D \quad (13)$$

where $\mathcal{M}_A = {}^h M_A + M_A$, $\mathcal{C}_A = {}^h C_A + C_A$, and $\mathcal{G}_A = {}^h G_A + G_A$.

B. Actuator Part

The joint dynamics of the robot in the presence of unmodeled dynamics in the actuator part and input constraints can be expressed as,

$$I_m \ddot{q} + \Delta_{\tau r} = \mathcal{B}_2(\tau^*) - \tau_m \quad (14)$$

where $\mathcal{B}_2(\cdot)$ is the internal combined input constraint in the sense of Lemma 4, with I_m being motor inertia, $\tau^* = \tau_i - \tau_{ai}$ being net control torque, where τ_i is control signal and τ_{ai} being defined later, and τ_m being interaction torque that derives human joint. Similar to (14), the human joint dynamics can be written as,

$$I_h \ddot{q} + \Delta_{\tau h} = \tau_m - \tau_h \quad (15)$$

where I_h is the equivalent inertia of the human joint and τ_h is human exogenous torque around the joint created by muscles. Substituting (15) into (14) and $\mathcal{B}_2(\tau^*) = \tau^* - \Delta \tau^*$ along with defining $\Delta_J = \Delta_{\tau h} + \Delta \tau^* + \Delta_{\tau r}$, we obtain,

$$\mathcal{I} \ddot{q} = \tau^* - \tau_h - \Delta_J \quad (16)$$

where $\mathcal{I} = I_m + I_h$.

The new equations specified in (13) and (16) are representations of rigid body and joint dynamics of the robot augmented with human arm link and joint dynamics in a decentralized way. In these equations, unmodeled dynamics in the actuator part and rigid body as well as in human arm is considered. In the following, a controller design procedure is explained.

IV. CONTROL DESIGN AND STABILITY PROOF

In the previous section, the decentralized dynamics of human arm and robot links in the presence of actuator constraints and model uncertainty are derived. In this section, a decentralized controller is designed to stabilize and accomplish the control objective of each subsystem. The decentralized scheme of the robot by means of VCPs and assigned VDC frames is illustrated in Fig. 2.

A. Rigid Body Part

As mentioned earlier, Δ_D is an unknown unmodeled dynamics that can be estimated by RBFNNs using Lemma 1,

$$\Delta_{Di} = W_{Di}^{*T} \Psi(\chi_{Di}) + \varepsilon_{Di}^* \quad (17)$$

where $i = 1, \dots, 7$, $W_{Di}^* \in \mathbb{R}^{j \times 6}$ is the optimal weights, $\chi_{Di} \in \mathbb{R}^j$ is the input, and $\varepsilon_{Di}^* = \bar{\varepsilon}_{Di}^* + F_{di}$ where $\bar{\varepsilon}_{Di}^* \in \mathbb{R}^6$ is the error vector of RBFNNs, and j is the number of neuron units in RBFNNs. Then, replacing A with B_i in (13) and utilizing the linear-in-parameter feature, one can write,

$$\mathcal{M}_{B_i} \frac{d}{dt}({}^{B_i} \mathcal{V}_r) + \mathcal{C}_{B_i}({}^{B_i} \mathcal{V}_r) + \mathcal{G}_{B_i} = Y_{B_i} \phi_{B_i} \quad (18)$$

where $i = 1, \dots, 7$, $Y_{B_i} \in \mathbb{R}^{6 \times 10}$ is the compact regressor matrix defined in [33] and $\phi_{B_i} \in \mathbb{R}^6$ are the constant inertial parameters. The following theorem summarizes the decentralized control and stability proof.

Theorem 2. For the decentralized model of pHRI with a rigid body part represented by the dynamic model of (13), the decentralized control action can be designed as,

$$\begin{aligned} {}^{B_i} \mathcal{F}_r^* &= \mathcal{K}_{Di} ({}^{B_i} \mathcal{V}_r - {}^{B_i} \mathcal{V}) + \hat{W}_{Di}^T \Psi(\chi_{Di}) + \hat{\varepsilon}_{Di} \\ &+ \mathcal{K}_{Ii} \int_0^t ({}^{B_i} \mathcal{V}_r - {}^{B_i} \mathcal{V}) dt + Y_{B_i} \hat{\phi}_{B_i} \end{aligned} \quad (19)$$

with the update rules as below,

$$\dot{\hat{\mathcal{L}}}_{B_i} = \frac{1}{\gamma_1} \hat{\mathcal{L}}_{B_i} \mathcal{S}_{B_i} \hat{\mathcal{L}}_{B_i} \quad (20)$$

$$\dot{\hat{W}}_{Di} = \Gamma_{B_i} \Psi(\chi_{Di}) ({}^{B_i} \mathcal{V}_r - {}^{B_i} \mathcal{V}) \quad (21)$$

$$\dot{\hat{\varepsilon}}_{Di} = \gamma_{2i} ({}^{B_i} \mathcal{V}_r - {}^{B_i} \mathcal{V}) \quad (22)$$

such that the virtual stability of the rigid body part is ensured in the sense of Definition 3. The $\hat{(\cdot)}$ denotes the estimated value, γ_1 and γ_{2i} are positive constants, and Γ_{B_i} are positive-definite constants. $\hat{\mathcal{L}}_{B_i}$ is derived from $\hat{\phi}_{B_i}$ utilizing Lemma 3.

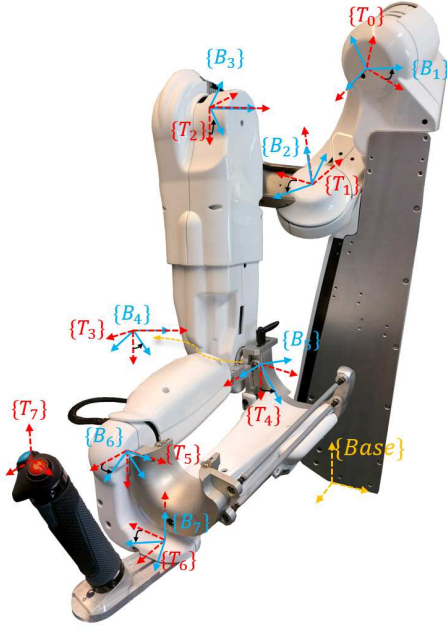


Fig. 2. VDC frames assigned to the upper limb exoskeleton

Proof. Replacing A with B_i in (13) and subtracting it from (19) and utilizing (17) and (18), we have,

$$\begin{aligned} {}^{B_i}\mathcal{F}_r^* - {}^{B_i}\mathcal{F}^* &= \mathcal{K}_{D_i}({}^{B_i}\mathcal{V}_r - {}^{B_i}\mathcal{V}) + Y_{B_i}\tilde{\phi}_{B_i} \\ &+ \mathcal{K}_{I_i} \int_0^t ({}^{B_i}\mathcal{V}_r - {}^{B_i}\mathcal{V}) dt + \tilde{W}_{D_i}^T \Psi(\chi_{D_i}) + \tilde{\varepsilon}_{D_i} \quad (23) \\ &+ \mathcal{M}_{B_i} \frac{d}{dt} ({}^{B_i}\mathcal{V}_r - {}^{B_i}\mathcal{V}) + \mathcal{C}_{B_i} ({}^{B_i}\mathcal{V}_r - {}^{B_i}\mathcal{V}) \end{aligned}$$

where $\tilde{(\cdot)} = \hat{(\cdot)} - (\cdot)^*$ for \tilde{W} and $\tilde{\varepsilon}$, and $\tilde{(\cdot)} = \hat{(\cdot)} - (\cdot)$ for $\tilde{\phi}$.

Based on Definition 1, the non-negative accompanying function candidate for stability analysis is,

$$\begin{aligned} v_i(t) &= \frac{1}{2} ({}^{B_i}\mathcal{V}_r - {}^{B_i}\mathcal{V})^T \mathcal{M}_{B_i} ({}^{B_i}\mathcal{V}_r - {}^{B_i}\mathcal{V}) \\ &+ \frac{1}{2} \left\{ \int_0^t ({}^{B_i}\mathcal{V}_r - {}^{B_i}\mathcal{V}) dt \right\}^T \mathcal{K}_{I_i} \left\{ \int_0^t ({}^{B_i}\mathcal{V}_r - {}^{B_i}\mathcal{V}) dt \right\} \\ &+ \gamma_1 \mathcal{D}_F(\mathcal{L}_{B_i} \| \hat{\mathcal{L}}_{B_i}) + \frac{1}{2} \text{tr}(\tilde{W}_{D_i}^T \Gamma_{B_i}^{-1} \tilde{W}_{D_i}) \\ &+ \frac{1}{2\gamma_{2i}} \tilde{\varepsilon}_{D_i}^T \tilde{\varepsilon}_{D_i}. \quad (24) \end{aligned}$$

where $\mathcal{D}_F(\mathcal{L}_{B_i} \| \hat{\mathcal{L}}_{B_i})$ defined as [33],

$$\mathcal{D}_F(\mathcal{L}_{B_i} \| \hat{\mathcal{L}}_{B_i}) = \log \frac{|\hat{\mathcal{L}}_{B_i}|}{|\mathcal{L}_{B_i}|} + \text{tr}(\hat{\mathcal{L}}_{B_i}^{-1} \mathcal{L}_{B_i}) - 4 \quad (25)$$

is the Bregman divergence metric. Taking the derivative of

(24) and using (23), leads to,

$$\begin{aligned} \dot{v}_i(t) &= ({}^{B_i}\mathcal{V}_r - {}^{B_i}\mathcal{V})^T ({}^{B_i}\mathcal{F}_r^* - {}^{B_i}\mathcal{F}^*) + \gamma_1 \text{tr}([\hat{\mathcal{L}}_{B_i}^{-1} \dot{\hat{\mathcal{L}}}_{B_i} \\ &\hat{\mathcal{L}}_{B_i}^{-1} \tilde{\mathcal{L}}_{B_i}) - ({}^{B_i}\mathcal{V}_r - {}^{B_i}\mathcal{V})^T \mathcal{K}_{D_i} ({}^{B_i}\mathcal{V}_r - {}^{B_i}\mathcal{V}) \\ &- ({}^{B_i}\mathcal{V}_r - {}^{B_i}\mathcal{V})^T Y_{B_i} \tilde{\phi}_{B_i} - ({}^{B_i}\mathcal{V}_r - {}^{B_i}\mathcal{V})^T \tilde{W}_{D_i}^T \Psi(\chi_{D_i}) \\ &- ({}^{B_i}\mathcal{V}_r - {}^{B_i}\mathcal{V})^T \tilde{\varepsilon}_{D_i} - ({}^{B_i}\mathcal{V}_r - {}^{B_i}\mathcal{V})^T \mathcal{C}_{B_i} ({}^{B_i}\mathcal{V}_r - {}^{B_i}\mathcal{V}) \\ &+ \frac{1}{\gamma_{2i}} \tilde{\varepsilon}_{D_i}^T \dot{\tilde{\varepsilon}}_{D_i} + \text{tr}(\tilde{W}_{D_i}^T \Gamma_{B_i}^{-1} \dot{\tilde{W}}_{D_i}). \quad (26) \end{aligned}$$

Recalling Lemma 3, defining $s_{B_i} = Y_{B_i}^T ({}^{B_i}\mathcal{V}_r - {}^{B_i}\mathcal{V})$, exploiting the relationship below,

$$({}^{B_i}\mathcal{V}_r - {}^{B_i}\mathcal{V})^T \tilde{W}_{D_i}^T \Psi(\chi_{D_i}) = \text{tr}(({}^{B_i}\mathcal{V}_r - {}^{B_i}\mathcal{V}) \Psi^T(\chi_{D_i}) \tilde{W}_{D_i})$$

and using $\tilde{\phi}_{B_i}^T s_{B_i} = \text{tr}(\tilde{\mathcal{L}}_{B_i} \mathcal{S}_{B_i})$, where \mathcal{S}_{B_i} is a unique symmetric matrix defined in Appendix A, along with the fact that \mathcal{C}_{B_i} is a skew-symmetric matrix, we can rewrite (26) as,

$$\begin{aligned} \dot{v}_i(t) &= ({}^{B_i}\mathcal{V}_r - {}^{B_i}\mathcal{V})^T ({}^{B_i}\mathcal{F}_r^* - {}^{B_i}\mathcal{F}^*) \\ &- \text{tr}(\{\mathcal{S}_{B_i} - \gamma_1 [\hat{\mathcal{L}}_{B_i}^{-1} \dot{\hat{\mathcal{L}}}_{B_i} \hat{\mathcal{L}}_{B_i}^{-1}]\} \tilde{\mathcal{L}}_{B_i}) \\ &- ({}^{B_i}\mathcal{V}_r - {}^{B_i}\mathcal{V})^T \mathcal{K}_{D_i} ({}^{B_i}\mathcal{V}_r - {}^{B_i}\mathcal{V}) \\ &- \text{tr}(\{({}^{B_i}\mathcal{V}_r - {}^{B_i}\mathcal{V}) \Psi^T(\chi_{D_i}) - \tilde{W}_{D_i}^T \Gamma_{B_i}^{-1}\} \tilde{W}_{D_i}) \\ &- \tilde{\varepsilon}_{D_i}^T (({}^{B_i}\mathcal{V}_r - {}^{B_i}\mathcal{V}) - \frac{1}{\gamma_{2i}} \tilde{\varepsilon}_{D_i}). \quad (27) \end{aligned}$$

Finally, by substituting (20)-(22) into (27), one can get,

$$\begin{aligned} \dot{v}_i(t) &= ({}^{B_i}\mathcal{V}_r - {}^{B_i}\mathcal{V})^T ({}^{B_i}\mathcal{F}_r^* - {}^{B_i}\mathcal{F}^*) \\ &- ({}^{B_i}\mathcal{V}_r - {}^{B_i}\mathcal{V})^T \mathcal{K}_{D_i} ({}^{B_i}\mathcal{V}_r - {}^{B_i}\mathcal{V}). \quad \blacksquare \quad (28) \end{aligned}$$

B. Actuator Dynamics Part

In this section, a control signal is designed to stabilize joint dynamics and obtain control goals. Because forces being engendered in muscles generate torques around joints, the estimation of the HEF is considered in the actuator dynamics part. Utilizing Lemma 1, Δ_j can be estimated as,

$$\Delta_j = W_{j_i}^{*T} \Psi(\chi_{j_i}) + \varepsilon_{j_i}^*. \quad (29)$$

where $i = 1, \dots, 7$, $W_{j_i}^* \in \mathfrak{R}^j$ is the optimal weights, $\chi_{D_i} \in \mathfrak{R}^j$ is the input, and $\varepsilon_{j_i}^* = \tilde{\varepsilon}_{j_i}^* + \tau_{h_i}$ where $\tilde{\varepsilon}_{j_i}^* \in \mathfrak{R}$ is the error vector of RBFNNs and τ_{h_i} is human exogenous torque represented at the i^{th} subsystem, where j is the number of neuron units in RBFNNs. In the next theorem, the control design and stability analysis of joint dynamics is examined.

Theorem 3. For the decentralized model of pHRI with actuator dynamics represented by the dynamic model of (16), the decentralized control action can be designed as,

$$\begin{aligned} \tau_{r_i}^* &= k_{d_i} (\dot{q}_{r_i} - \dot{q}_i) + k_{I_i} \int_0^t (\dot{q}_{r_i} - \dot{q}_i) dt \\ &+ Y_{a_i} \hat{\phi}_{a_i} + \hat{W}_{j_i}^T \Psi(\chi_{j_i}) + \hat{\varepsilon}_{j_i} + \frac{e_{a_i}}{k_{b_i}^2 - e_{a_i}^2} \quad (30) \end{aligned}$$

with the update rules as follows:

$$\dot{\hat{\mathcal{L}}}_{a_i} = \frac{1}{\zeta} \hat{\mathcal{L}}_{a_i} \mathcal{S}_{a_i} \hat{\mathcal{L}}_{a_i} \quad (31)$$

$$\dot{W}_{Ji} = \beta_{1i} (\dot{q}_{ri} - \dot{q}_i) \Psi(\chi_{Ji}) \quad (32)$$

$$\dot{\hat{\epsilon}}_{Ji} = \beta_{2i} (\dot{q}_{ri} - \dot{q}_i) \quad (33)$$

such that the virtual stability of the rigid body part is ensured in the sense of Definition 3. The (\cdot) denotes the estimated value, ζ , β_{1i} , and β_{2i} are positive constants. $\hat{\mathcal{L}}_{ai}$ is derived from $\hat{\phi}_{ai}$ utilizing Lemma 3. Moreover, $e_a = q_r - q$ and k_{bi} are in the sense of Lemma 2.

Proof. Subtracting (16) from (30) and using (29), we have,

$$\begin{aligned} \tau_{ri}^* - \tau_i^* &= k_{di}(\dot{q}_{ri} - \dot{q}_i) + k_{Ii} \int_0^t (\dot{q}_{ri} - \dot{q}_i) dt + Y_{ai} \tilde{\phi}_{ai} \\ &+ \tilde{W}_{Ji}^T \Psi(\chi_{Ji}) + \tilde{\epsilon}_{Ji} + \mathcal{I} \frac{d}{dt} (\dot{q}_{ri} - \dot{q}_i) + \frac{e_{ai}}{k_{bi}^2 - e_{ai}^2}. \end{aligned} \quad (34)$$

Then, the accompanying function corresponding to the actuator part can be defined as,

$$\begin{aligned} \nu_{ai}(t) &= \frac{1}{2} \mathcal{I} (\dot{q}_{ri} - \dot{q}_i) + \frac{1}{2} k_{Ii} \left\{ \int_0^t (\dot{q}_{ri} - \dot{q}_i) dt \right\}^2 \\ &+ \zeta \mathcal{D}_F(\mathcal{L}_{ai} \| \hat{\mathcal{L}}_{ai}) + \frac{1}{2\beta_{2i}} \tilde{\epsilon}_{Ji}^2 + \frac{1}{2\beta_{1i}} \tilde{W}_{Ji}^T \tilde{W}_{Ji} \quad (35) \\ &+ \frac{1}{2} \log \frac{k_{bi}^2}{k_{bi}^2 - e_{ai}^2}. \end{aligned}$$

where $\mathcal{D}_F(\mathcal{L}_{ai} \| \hat{\mathcal{L}}_{ai})$ is defined the same as (25). Taking the derivative of (35) and using (34), one can obtain,

$$\begin{aligned} \dot{\nu}_{ai}(t) &= (\dot{q}_{ri} - \dot{q}_i)(\tau_{ri}^* - \tau_i^*) + \zeta \text{tr}([\hat{\mathcal{L}}_{ai}^{-1} \dot{\hat{\mathcal{L}}}_{ai} \hat{\mathcal{L}}_{ai}^{-1}] \tilde{\mathcal{L}}_{ai}) \\ &- k_{di}(\dot{q}_{ri} - \dot{q}_i)^2 - (\dot{q}_{ri} - \dot{q}_i) Y_{ai} \tilde{\phi}_{ai} + \frac{\dot{e}_{ai} e_{ai}}{k_{bi}^2 - e_{ai}^2} \\ &- (\dot{q}_{ri} - \dot{q}_i) \tilde{W}_{Ji}^T \Psi(\chi_{Ji}) - (\dot{q}_{ri} - \dot{q}_i) \tilde{\epsilon}_{Ji} \\ &- (\dot{q}_{ri} - \dot{q}_i) \frac{e_{ai}}{k_{bi}^2 - e_{ai}^2} + \frac{1}{\beta_{2i}} \tilde{\epsilon}_{Ji} \dot{\tilde{\epsilon}}_{Ji} + \frac{1}{\beta_{1i}} \dot{\tilde{W}}_{Ji}^T \tilde{W}_{Ji}. \end{aligned} \quad (36)$$

Now, by defining $s_{ai} = Y_{ai}^T (\dot{q}_{ri} - \dot{q}_i)$, replacing (31)-(33) in (36), and using the fact that $\dot{e}_a = \dot{q}_r - \dot{q}$, we get to,

$$\dot{\nu}_{ai}(t) = (\dot{q}_{ri} - \dot{q}_i)(\tau_{ri}^* - \tau_i^*) - k_{di}(\dot{q}_{ri} - \dot{q}_i)^2. \quad \blacksquare \quad (37)$$

In the control signal (30), the last term is related to the state constraint, which is derived from the logarithmic Lyapunov function. In this constraint term, defining error based on the required angle applies much stricter control action to avoid violating the constraints, resulting in nearly zero tracking error. Moreover, human exogenous torque τ_{hi} is estimated along with the error vector of RBFNNs.

C. Control Signal

Thus far, the required net torques and forces for joints and rigid bodies, respectively, are designed which makes them behave in a desired way. In this part, the unified control command that will be transmitted to the motor is derived. The unified control signal can be computed as below,

$$\tau_i = \tau_{ri}^* + \tau_{ari} \quad (38)$$

where τ_{ri}^* is defined in (30) and τ_{ari} is a term related to rigid body dynamics, which is computed in this section.

The linear/angular velocity vectors can be computed using kinematic relationships as,

$$B_i \mathcal{V} = {}^{T_{i-1}}U_{B_i}^T {}^{T_{i-1}}\mathcal{V} + \mu_i \dot{q}_i \quad (39)$$

$${}^{T_i}\mathcal{V} = B_i U_{T_i}^T B_i \mathcal{V} \quad (40)$$

where $i = 1 \dots 7$, and ${}^{T_0}\mathcal{V} = {}^G\mathcal{V}$ and ${}^{T_7}\mathcal{V}$ are the linear/angular velocity vector of the ground and end-effector, respectively, q_i and \dot{q}_i are the joint angles and velocities, respectively, $\mu_i = z_\tau$ for $i = 1, 2, 3, 4, 6$, $\mu_i = y_\tau$ for $i = 7$, and $\mu_i = x_\tau$ for $i = 5$, which $z_\tau = [0, 0, 0, 0, 0, 1]^T$, $y_\tau = [0, 0, 0, 0, 1, 0]^T$, and $x_\tau = [0, 0, 0, 1, 0, 0]^T$. Moreover, ${}^{B_i}U_{T_i}$ can be computed with (1) by replacing B and A with T_i and B_i , respectively. The required linear/angular velocities can also be expressed as

$${}^{B_i}\mathcal{V}_r = {}^{T_{i-1}}U_{B_i}^T {}^{T_{i-1}}\mathcal{V}_r + \mu_i \dot{q}_{ri} \quad (41)$$

$${}^{T_i}\mathcal{V}_r = B_i U_{T_i}^T B_i \mathcal{V}_r \quad (42)$$

where ${}^{T_0}\mathcal{V}_r = {}^G\mathcal{V}_r$ and ${}^{T_7}\mathcal{V}_r$ are the required linear/angular velocity vectors of the ground and end-effector, respectively, and \dot{q}_{ri} is the required joint angular velocity defined as,

$$\dot{q}_{ri} = \dot{q}_{di} + \lambda_i (q_{di} - q_i) \quad (43)$$

where λ_i are positive constants. The required linear/angular velocity vectors defined in (41) are used in the control action of (19) to compute the net required force/moment vector.

Then, the force/moment vectors can be calculated as,

$${}^{B_j}\mathcal{F} = B_j U_{T_j}^T T_j \mathcal{F} + B_j \mathcal{F}^* \quad (44)$$

$${}^{T_{j-1}}\mathcal{F} = T_{j-1} U_{B_j} B_j \mathcal{F} \quad (45)$$

with required terms as,

$${}^{B_j}\mathcal{F}_r = B_j U_{T_j}^T T_j \mathcal{F}_r + B_j \mathcal{F}_r^* \quad (46)$$

$${}^{T_{j-1}}\mathcal{F}_r = T_{j-1} U_{B_j} B_j \mathcal{F}_r \quad (47)$$

where ${}^{T_7}\mathcal{F}$ is the interaction force between the end-effector and environment, and ${}^{T_0}\mathcal{F}$ is the applied force from joint 1 to the ground for $j = 7 \dots 1$. ${}^{B_j}\mathcal{F}_r^*$ is the required net force/moment vector defined in (19). Therefore, the second term in (38) can be computed as,

$$\tau_{ari} = \mu_i^T B_i \mathcal{F}_r. \quad (48)$$

with $i = 1 \dots 7$. In the following, the final theorem for stability analysis of the entire system is provided.

Theorem 4. The entire pHRI model, which is represented by (13) and (16) in the decentralized model, is asymptotically stable in the sense of Theorem 1 under the control action of (38) with update laws of (20)-(22) and (31)-(33).

Proof. See Appendix B.

Remark 2. τ_i is the control signal that is applied to the system and is exposed to \mathfrak{B}_i , the constraint function containing a dead zones and saturation. Then, the internal constraint functions, \mathcal{B}_{1i} and \mathcal{B}_{2i} , are subjected to the conditions below,

$$\min \mathfrak{B}_i = \min \mathcal{B}_{1i} + \min \mathcal{B}_{2i}$$

$$\max \mathfrak{B}_i = \max \mathcal{B}_{1i} + \max \mathcal{B}_{2i}.$$

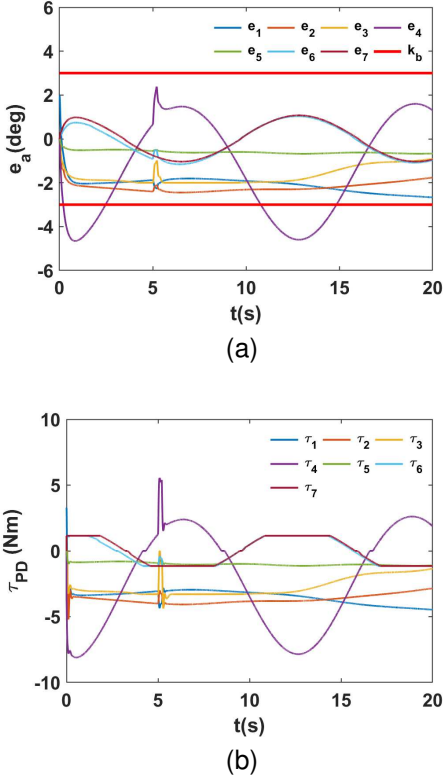


Fig. 3. PD control results in simulation. a) trajectory tracking error, b) control action

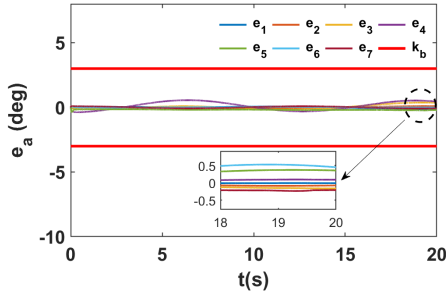


Fig. 4. Required joint angle error with proposed controller in simulation

V. RESULTS

In this section, the numerical and experimental results are provided to evaluate the proposed neuro-adaptive decentralized controller. The numerical analysis is performed by utilizing SIMULINK. Experiments, however, are performed using the commercial 7 DoF upper-limb exoskeleton ABLE. All high-level processes are accomplished in a host computer, and computed torque signals are transmitted to the robot using SIMULINK and the Virtuose interface, provided by Haption, with a sample time of 1 ms. In simulation and experiment, for the first three joints and fifth joint, the set point reaching control goal is examined, while for the fourth and last two joints, the trajectory tracking control goal is considered. This practice can be seen as both passive rehabilitation of forearm and wrist in medical applications and heavy object manipulation in industrial applications. Moreover, the result of the

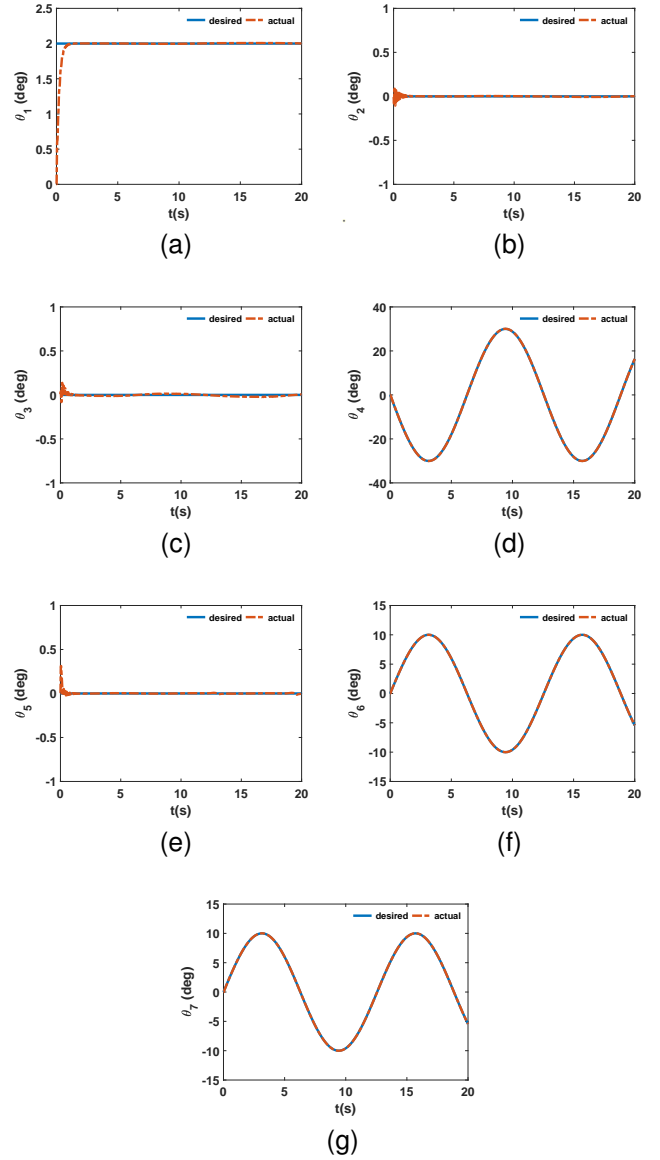


Fig. 5. Desired trajectory tracking of all joints in simulation

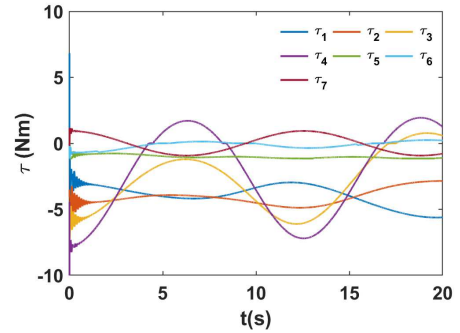


Fig. 6. Time history of Proposed control signal in simulation

proportional-derivative (PD) controller, defining as

$$\tau_{PD} = k_{pi}(q_{di} - q_i) + k_{vi}(\dot{q}_{di} - \dot{q}_i) \quad (49)$$

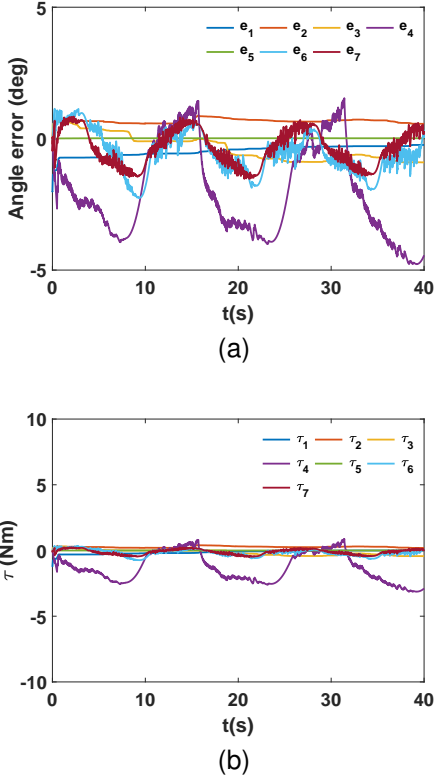


Fig. 7. Experimental results of PD control, a) desired trajectory tracking error, b) control torque

TABLE I
CONTROL PARAMETERS FOR SIMULATION

Symbol	Value	Symbol	Value
λ_i	5	\mathcal{K}_{Di}	$3\mathbf{I}_{6 \times 6}$
\mathcal{K}_{Ii}	$5\mathbf{I}_{6 \times 6}$	Γ_{Bi}	$10\mathbf{I}_{9 \times 9}$
γ_1	10	γ_{2i}	10
k_{di}	1.5	k_{Ii}	5
ζ	10	β_{1i}	10
β_{2i}	10	k_{pi}	100
k_{vi}	15	k_{bi}	3(deg)

where k_{pi} and k_{vi} are positive constants, is provided and compared with the proposed controller. The radial basis function for RBFNN is chosen as Gaussian function described as $\Psi_j(\chi) = \exp[-(\chi - c_j)^T(\chi - c_j)/(b_j^2)]$, with c_j and b_j denoting the center and width of the neural cell in j th unit. In this study the value for c_j is randomly selected in $[-1, 1]$ and $b_j = 1$ for $j = 1, \dots, 9$. The input vectors are $\chi_{Di} = [{}^{B_i}\mathcal{V}_r, {}^{B_i}\mathcal{V}, {}^{B_i}E_I, {}^{B_i}E_D, \tau_{ari}]^T$ and $\chi_{Ji} = [\dot{q}_{ri}, \dot{q}_{ri}, \dot{q}_i, e_{ai}, \dot{e}_{ai}, \tau_{ri}^*]^T$, where ${}^{B_i}E_I = \int_0^t ({}^{B_i}\mathcal{V}_r - {}^{B_i}\mathcal{V})dt$, ${}^{B_i}E_D = {}^{B_i}\mathcal{V}_r - {}^{B_i}\mathcal{V}$.

A. Numerical Results

In this section the simulation results are utilized to examine the performance of the proposed controller. For this aim, the desired trajectory for the joints are, $\mathbf{q}_d(t) = [0.035, 0, 0, -0.52 \sin 0.5t, 0, 0.175 \sin 0.5t, 0.175 \sin 0.5t]^T$ (rad) with the initial value of $[0, 0, 0, 0, 0, 0, 0]^T$. The force disturbances applied to each link are, $\mathbf{F}_d(t)(N) = [5 \sin 0.2t, 5 \sin 0.2t, 5 \sin 0.2t, 5 \sin 0.1t, 3 \sin 0.1t, 3 \sin 0.1t]^T$.

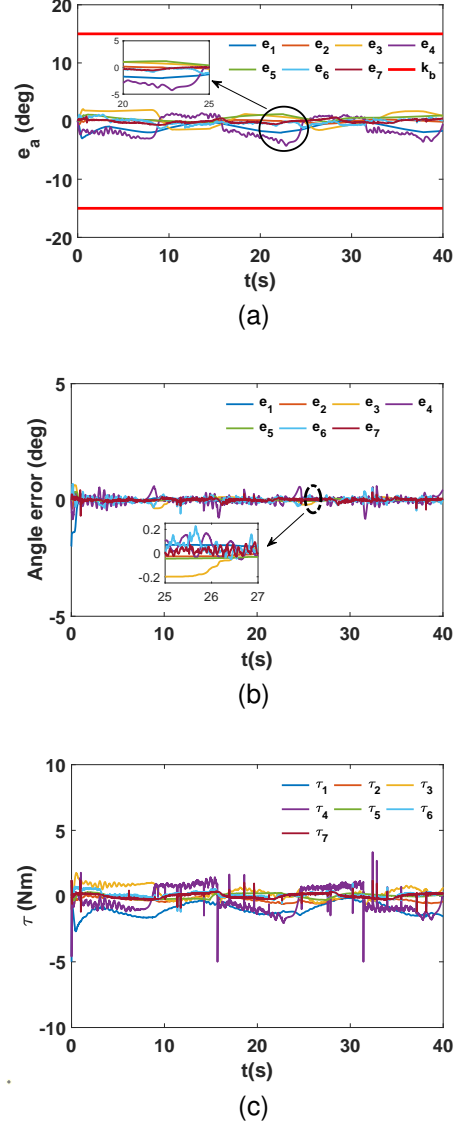


Fig. 8. Experimental results of proposed controller, a) time history of required joint error e_a , b) desired trajectory tracking error, c) time history of control torque applied to robot

The base of the exoskeleton is fixed and the end-effector has no contact with environment, implicating ${}^G\mathcal{V}, {}^{T_7}\mathcal{V} = \mathbf{0}_{6 \times 1}$. The constraint limit k_{bi} is selected to be 3 degrees for the simulation part. The selected control parameters for simulation are shown in Table 1. Additionally, the saturation level for the robot joints is $\pm 12N \cdot m$ for the first four joints and $\pm 1.2N \cdot m$ for last three joints. The dead zones offset is also ± 0.2 for first four joints and ± 0.05 for last three joints.

Fig. 3 demonstrates PD control results for the control of 7 DoF upper limb exoskeleton. Fig. 3(a) shows the trajectory tracking error, while Fig. 3(b) displays the applied control torque to the exoskeleton in order to follow the desired trajectory. As it can be seen, the tracking error under PD control law is large, and the states constraints are violated. Accordingly, PD controller cannot handle the unknown disturbance and nonlinearity of 7 DoF exoskeleton in presence of input constraints.

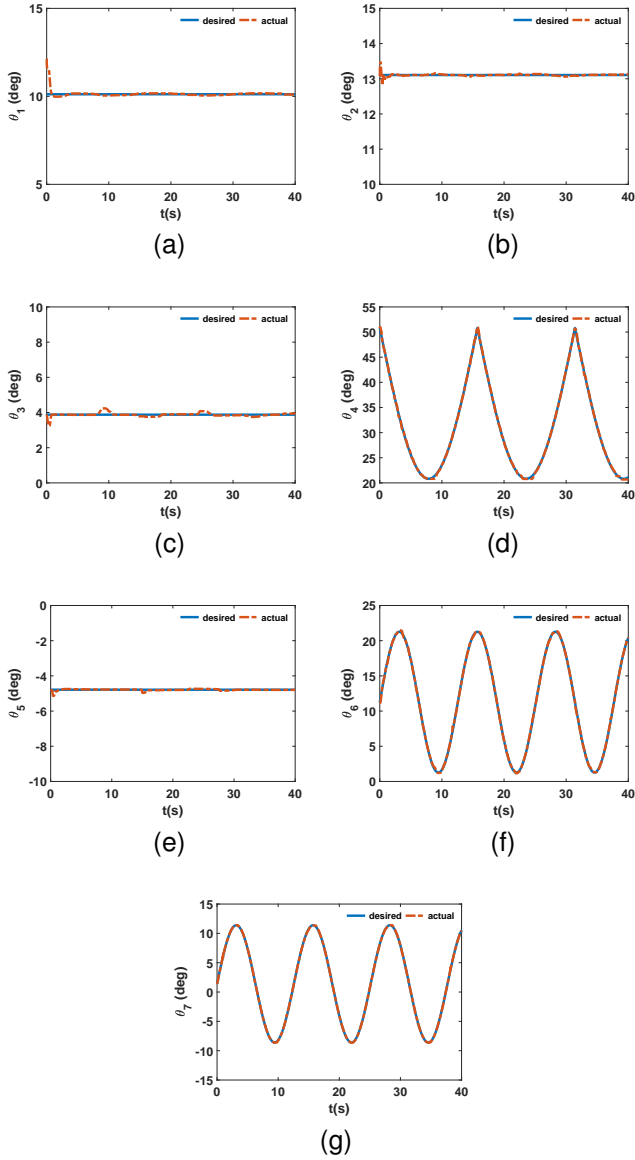


Fig. 9. Experimental results of desired trajectory tracking with proposed controller

The numerical results of the proposed controller are presented in Figs. 4-6. Fig. 4 demonstrates the required joint angle error e_a , based on which the constraint term is defined in (30). As it can be seen, not only the proposed controller maintained the e_a in the constrained domain with no violation, but it also resulted in a nearly zero value for e_a . This shows the excellent performance of the designed controller in cancelling all the nonlinearities of the high DoF system in presence of actuator and model uncertainty along with unknown actuator constraints. Moreover, an unknown disturbance is handled by the proposed controller. Fig. 5 displays the perfect trajectory tracking for exoskeleton. Fig. 6, however, shows the torque signal applied to each joint. Comparing Fig. 3(b) and Fig. 6, it can be concluded that the proposed controller accomplished control objectives without reaching the saturation level, whereas PD controller did not show good performance

although it reached the saturation level.

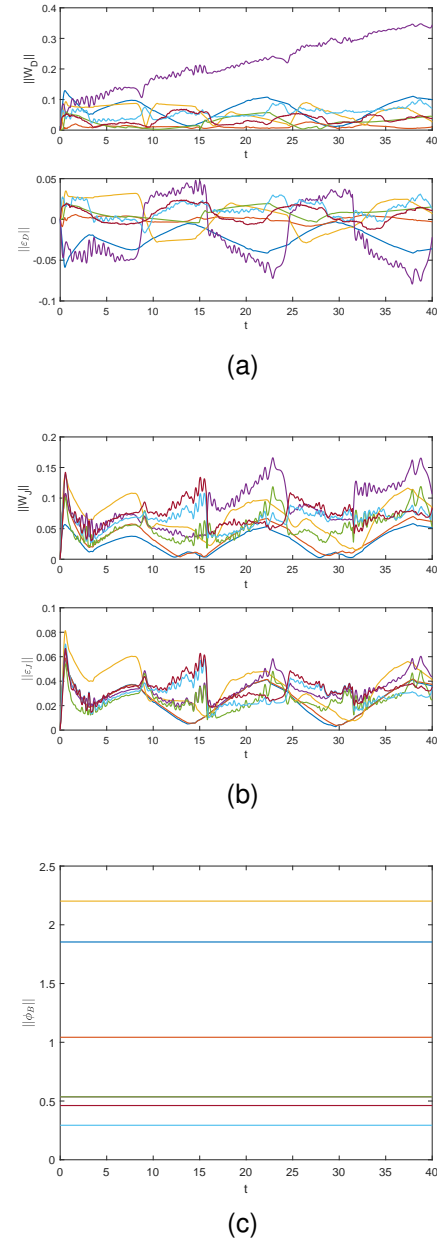


Fig. 10. Time history of the estimated parameters, a) norm of the weight and error vector of the NN related to rigid body, b) norm of the weight and error vector of the NN related to joints, c) norm of the estimated rigid body parameters

B. Experimental Results

To perform experiments and analyze the performance of the designed control method, the commercial exoskeleton ABLE is utilized. The selected control parameters are presented in Table. 2. In order to prevent fluctuations in the control torque resulting from the numerical calculation of the last term in (30), the constraint limit k_{bi} is set to 15 degrees. However, as the constraint term is defined based on the required tracking error e_a in (30), the desired tracking error is nearly zero. In the experiment, an unknown external disturbance is applied to

TABLE II
CONTROL PARAMETERS FOR EXPERIMENT

Symbol	Value	Symbol	Value
λ_i	6	\mathcal{K}_{D1}	$0.2\mathbb{I}_{6 \times 6}$
\mathcal{K}_{D2}	$0.2\mathbb{I}_{6 \times 6}$	\mathcal{K}_{D3}	$0.2\mathbb{I}_{6 \times 6}$
\mathcal{K}_{D4}	$0.7\mathbb{I}_{6 \times 6}$	\mathcal{K}_{D5}	$0.2\mathbb{I}_{6 \times 6}$
\mathcal{K}_{D6}	$0.3\mathbb{I}_{6 \times 6}$	\mathcal{K}_{D7}	$0.2\mathbb{I}_{6 \times 6}$
\mathcal{K}_{Ii}	$2\mathbb{I}_{6 \times 6}$	Γ_{Bi}	$2\mathbb{I}_{9 \times 9}$
γ_1	10	γ_{2i}	1
k_{di}	0.05	k_{Ii}	2
ζ	10	β_{1i}	2
β_{2i}	1	k_{pi}	40
k_{vi}	0.5	k_{bi}	15(deg)

the exoskeleton while it is performing the task. The saturation level for the first four motors is $\pm 5N \cdot m$ and for the last three joints $\pm 1.2N \cdot m$. The dead zone parameters are the same as those in the simulation. Moreover, the control goal for the second, third, and fifth joints is to stay in the initial state, while joint four and the last two joints have to track the desired trajectory. In order to keep the first joint away from its mechanical range limit, it should reach *initial_point - 2degree* point. The results of PD control law and designed controller are compared to demonstrate the performance of the presented control scheme.

Fig. 7 depicts the experimental results of PD controller. Fig. 7(a) shows the trajectory tracking error and Fig. 7(b) displays the control action produced by PD control law and applied to the exoskeleton. As shown in Fig. 7(a), the tracking error is large, and PD controller does not perform well. Moreover, for those joints with set point reaching goal, there are steady state errors.

The experimental results of applying the designed controller to the exoskeleton is provided in Fig. 8. In Fig. 8(a), the required joint angle error e_a is displayed, Fig. 8(b) shows the desired trajectory tracking error of joints, and Fig. 8(c) demonstrates the produced control torque that is conveyed to exoskeleton. As is evident from Fig. 8(a), the value of e_a is less than 5 degrees. Despite the selected value for k_{bi} in the experiment, as previously mentioned, designing the constraint term in (30) based on the required joint error e_a applies an intense constraint to the joint tracking error. This can be seen from Fig. 8(b), where the tracking error for all joints is nearly zero and there is no steady state error for joints with set point reaching goal. All the mentioned achievements are accomplished by consuming less than $2N \cdot m$ torque, according to Fig. 8(c). Moreover, the sharp points in Fig. 8(c) correspond to unknown disturbance rejection. Fig. 9, moreover, shows the experimental results of trajectory tracking and set point reaching for each joint of upper limb exoskeleton. Taken together, the designed neuro-adaptive decentralized controller has demonstrated excellent performance in disturbance rejection, nonlinearity canceling, stabilizing the whole system, and handling unknown model and actuator uncertainty. Having a very small tracking error with required low control torque along with an excellent ability to reject disturbances, the proposed controller perfectly ensures physical safety in pHRI.

As a final figure, Fig. 10 depicts the norm of updated neural networks weights and approximation error vectors along with

the estimation of unknown rigid body parameters. Fig. 10(a) shows the norm of the updated weights and error vector for all the rigid bodies, Fig. 10(b) displays the norm of the updated weights and error vector for all the joints, and Fig. 10(c) demonstrates the norm of the estimated unknown parameters of all rigid bodies. As these figures illustrate, all the norms are bound.

VI. CONCLUSION

Considering the safety of human operator in physical human-robot interaction of upper limb exoskeleton, this study designed an RBFNN-based adaptive decentralized controller that ensures the safety of human operator by considering unknown robot and human model uncertainty, actuator dynamics constraints and uncertainty, along with unknown disturbance rejection. The Employed VDC scheme helped to break down the entire complex system into subsystems and design the controller at the subsystem level. The changes in control action of each subsystem do not affect other subsystems, resulting in a robust control method. In addition, estimating human exogenous force and inertial parameter of human arm and considering them in the control law increased the performance of designed controller and made it adaptable for different human operator. In order to apply constraints on states and guarantee physical safety, the control law is modified using the barrier Lyapunov function. Stability of the entire system under designed control law is analysed by means of virtual stability and VPFs, and the asymptotic stability is established. Finally, both the numerical and experimental results are exploited to examine the performance of designed controller. As it can be concluded from the results section, the proposed controller demonstrated excellent performance in stabilizing the system and accomplishing the control objectives. Moreover, the numerical and experimental results of PD controller are utilized to compare it with proposed controller. Results display that the proposed controller establishes the control objectives with nearly zero error and requires low torque, which ensures the physical safety of human operator and outperforms PD control method.

VII. APPENDIX

A. Defining \mathcal{S}_{B_i}

The standard inner product defined between the inertial parameter vector $\phi_{B_i} \in \mathbb{R}^{10}$ and a coefficient vector $s_{B_i} \in \mathbb{R}^{10}$ can be uniquely restated as the trace product between pseudo inertia matrix and some 4×4 symmetric matrix as,

$$\phi_{B_i}^T s_{B_i} = \text{tr}(\mathcal{L}_{B_i} \mathcal{S}_{B_i}(s_{B_i}))$$

with

$$\mathcal{S}_{B_i}(s) = \begin{bmatrix} s_6 + s_7 & -0.5s_8 & -0.5s_{10} & 0.5s_2 \\ -0.5s_8 & s_5 + s_7 & -0.5s_9 & 0.5s_3 \\ -0.5s_{10} & -0.5s_9 & s_5 + s_6 & 0.5s_4 \\ 0.5s_2 & 0.5s_3 & 0.5s_4 & s_1 \end{bmatrix}.$$

B. Proof of Theorem 4

In order to prove Theorem 4, we need to rewrite the first terms of (28) and (37) for $i = 1, \dots, 7$. It follows from (3), (7), (44),

$$\begin{aligned} (B_1 \mathcal{V}_r - B_1 \mathcal{V})^T (B_1 \mathcal{F}_r^* - B_1 \mathcal{F}^*) &= (B_1 \mathcal{V}_r - B_1 \mathcal{V})^T \\ (B_1 \mathcal{F}_r - B_1 \mathcal{F}) - (B_1 U_{T1}^T (B_1 \mathcal{V}_r - B_1 \mathcal{V}))^T & \\ (B_1 \mathcal{F}_r - B_1 \mathcal{F}) &= (B_1 \mathcal{V}_r - B_1 \mathcal{V})^T (B_1 \mathcal{F}_r - B_1 \mathcal{F}) \\ - (T_1 \mathcal{V}_r - T_1 \mathcal{V})^T (T_1 \mathcal{F}_r - T_1 \mathcal{F}) &= p_{B1} - p_{T1}. \end{aligned} \quad (I.1)$$

In the same way, we have for all the frames,

$$\begin{aligned} (B_2 \mathcal{V}_r - B_2 \mathcal{V})^T (B_2 \mathcal{F}_r^* - B_2 \mathcal{F}^*) &= (B_2 \mathcal{V}_r - B_2 \mathcal{V})^T \\ (B_2 \mathcal{F}_r - B_2 \mathcal{F}) - (T_2 \mathcal{V}_r - T_2 \mathcal{V})^T (T_2 \mathcal{F}_r - T_2 \mathcal{F}) & \\ = p_{B2} - p_{T2} & \end{aligned} \quad (I.2)$$

$$\begin{aligned} (B_3 \mathcal{V}_r - B_3 \mathcal{V})^T (B_3 \mathcal{F}_r^* - B_3 \mathcal{F}^*) &= (B_3 \mathcal{V}_r - B_3 \mathcal{V})^T \\ (B_3 \mathcal{F}_r - B_3 \mathcal{F}) - (T_3 \mathcal{V}_r - T_3 \mathcal{V})^T (T_3 \mathcal{F}_r - T_3 \mathcal{F}) & \\ = p_{B3} - p_{T3} & \end{aligned} \quad (I.3)$$

$$\begin{aligned} (B_4 \mathcal{V}_r - B_4 \mathcal{V})^T (B_4 \mathcal{F}_r^* - B_4 \mathcal{F}^*) &= (B_4 \mathcal{V}_r - B_4 \mathcal{V})^T \\ (B_4 \mathcal{F}_r - B_4 \mathcal{F}) - (T_4 \mathcal{V}_r - T_4 \mathcal{V})^T (T_4 \mathcal{F}_r - T_4 \mathcal{F}) & \\ = p_{B4} - p_{T4} & \end{aligned} \quad (I.4)$$

$$\begin{aligned} (B_5 \mathcal{V}_r - B_5 \mathcal{V})^T (B_5 \mathcal{F}_r^* - B_5 \mathcal{F}^*) &= (B_5 \mathcal{V}_r - B_5 \mathcal{V})^T \\ (B_5 \mathcal{F}_r - B_5 \mathcal{F}) - (T_5 \mathcal{V}_r - T_5 \mathcal{V})^T (T_5 \mathcal{F}_r - T_5 \mathcal{F}) & \\ = p_{B5} - p_{T5} & \end{aligned} \quad (I.5)$$

$$\begin{aligned} (B_6 \mathcal{V}_r - B_6 \mathcal{V})^T (B_6 \mathcal{F}_r^* - B_6 \mathcal{F}^*) &= (B_6 \mathcal{V}_r - B_6 \mathcal{V})^T \\ (B_6 \mathcal{F}_r - B_6 \mathcal{F}) - (T_6 \mathcal{V}_r - T_6 \mathcal{V})^T (T_6 \mathcal{F}_r - T_6 \mathcal{F}) & \\ = p_{B6} - p_{T6} & \end{aligned} \quad (I.6)$$

$$\begin{aligned} (B_7 \mathcal{V}_r - B_7 \mathcal{V})^T (B_7 \mathcal{F}_r^* - B_7 \mathcal{F}^*) &= (B_7 \mathcal{V}_r - B_7 \mathcal{V})^T \\ (B_7 \mathcal{F}_r - B_7 \mathcal{F}) - (T_7 \mathcal{V}_r - T_7 \mathcal{V})^T (T_7 \mathcal{F}_r - T_7 \mathcal{F}) & \\ = p_{B7} - p_{T7}. & \end{aligned} \quad (I.7)$$

By subtracting $\tau^* = \tau_i - \tau_{ai}$ from (38), one can write,

$$\tau_{ri}^* - \tau_i^* = -(\tau_{ri} - \tau_i). \quad (I.8)$$

Then, utilizing (3), (7), and (39), we can write the first term of (37) as,

$$\begin{aligned} (\dot{q}_{r1} - \dot{q}_1)(\tau_{r1}^* - \tau_1^*) &= -(\dot{q}_{r1} - \dot{q}_1)(\tau_{r1} - \tau_1) = \\ - ((B_1 \mathcal{V}_r - B_1 \mathcal{V}) - T_0 U_{B1}^T (T_0 \mathcal{V}_r - T_0 \mathcal{V}))^T & \\ (B_1 \mathcal{F}_r - B_1 \mathcal{F}) &= -(B_1 \mathcal{V}_r - B_1 \mathcal{V})^T (B_1 \mathcal{F}_r - B_1 \mathcal{F}) \\ + (T_0 \mathcal{V}_r - T_0 \mathcal{V})^T (T_0 \mathcal{F}_r - T_0 \mathcal{F}) &= -p_{B1} + p_{T0}. \end{aligned} \quad (I.9)$$

In the same way, it can be done for all the joints,

$$\begin{aligned} (\dot{q}_{r2} - \dot{q}_2)(\tau_{r2}^* - \tau_2^*) &= -(\dot{q}_{r2} - \dot{q}_2)(\tau_{r2} - \tau_2) = \\ - (B_2 \mathcal{V}_r - B_2 \mathcal{V})^T (B_2 \mathcal{F}_r - B_2 \mathcal{F}) & \\ + (T_1 \mathcal{V}_r - T_1 \mathcal{V})^T (T_1 \mathcal{F}_r - T_1 \mathcal{F}) &= -p_{B2} + p_{T1}. \end{aligned} \quad (I.10)$$

$$\begin{aligned} (\dot{q}_{r3} - \dot{q}_3)(\tau_{r3}^* - \tau_3^*) &= -(\dot{q}_{r3} - \dot{q}_3)(\tau_{r3} - \tau_3) = \\ - (B_3 \mathcal{V}_r - B_3 \mathcal{V})^T (B_3 \mathcal{F}_r - B_3 \mathcal{F}) & \\ + (T_2 \mathcal{V}_r - T_2 \mathcal{V})^T (T_2 \mathcal{F}_r - T_2 \mathcal{F}) &= -p_{B3} + p_{T2}. \end{aligned} \quad (I.11)$$

$$\begin{aligned} (\dot{q}_{r4} - \dot{q}_4)(\tau_{r4}^* - \tau_4^*) &= -(\dot{q}_{r4} - \dot{q}_4)(\tau_{r4} - \tau_4) = \\ - (B_4 \mathcal{V}_r - B_4 \mathcal{V})^T (B_4 \mathcal{F}_r - B_4 \mathcal{F}) & \\ + (T_3 \mathcal{V}_r - T_3 \mathcal{V})^T (T_3 \mathcal{F}_r - T_3 \mathcal{F}) &= -p_{B4} + p_{T3}. \end{aligned} \quad (I.12)$$

$$\begin{aligned} (\dot{q}_{r5} - \dot{q}_5)(\tau_{r5}^* - \tau_5^*) &= -(\dot{q}_{r5} - \dot{q}_5)(\tau_{r5} - \tau_5) = \\ - (B_5 \mathcal{V}_r - B_5 \mathcal{V})^T (B_5 \mathcal{F}_r - B_5 \mathcal{F}) & \\ + (T_4 \mathcal{V}_r - T_4 \mathcal{V})^T (T_4 \mathcal{F}_r - T_4 \mathcal{F}) &= -p_{B5} + p_{T4}. \end{aligned} \quad (I.13)$$

$$\begin{aligned} (\dot{q}_{r6} - \dot{q}_6)(\tau_{r6}^* - \tau_6^*) &= -(\dot{q}_{r6} - \dot{q}_6)(\tau_{r6} - \tau_6) = \\ - (B_6 \mathcal{V}_r - B_6 \mathcal{V})^T (B_6 \mathcal{F}_r - B_6 \mathcal{F}) & \\ + (T_5 \mathcal{V}_r - T_5 \mathcal{V})^T (T_5 \mathcal{F}_r - T_5 \mathcal{F}) &= -p_{B6} + p_{T5}. \end{aligned} \quad (I.14)$$

$$\begin{aligned} (\dot{q}_{r7} - \dot{q}_7)(\tau_{r7}^* - \tau_7^*) &= -(\dot{q}_{r7} - \dot{q}_7)(\tau_{r7} - \tau_7) = \\ - (B_7 \mathcal{V}_r - B_7 \mathcal{V})^T (B_7 \mathcal{F}_r - B_7 \mathcal{F}) & \\ + (T_6 \mathcal{V}_r - T_6 \mathcal{V})^T (T_6 \mathcal{F}_r - T_6 \mathcal{F}) &= -p_{B7} + p_{T6}. \end{aligned} \quad (I.15)$$

Now, the general accompanying function can be defined as,

$$\nu(t) = \sum_1^7 (\nu_i(t) + \nu_{ai}(t)) \quad (I.16)$$

and taking time derivative of (I.16) and using (28), (37), and (I.1)-(I.15), leads to,

$$\begin{aligned} \dot{\nu}(t) = - \sum_1^7 (k_{di}(\dot{q}_r - \dot{q}_i)^2 + (B_i \mathcal{V}_r - B_i \mathcal{V})^T \mathcal{K}_{Di} & \\ (B_i \mathcal{V}_r - B_i \mathcal{V})) \leq 0. & \end{aligned} \quad (I.17)$$

It can be seen that all the VPFs cancelled each other, and asymptotic stability of the entire system under the designed decentralized controller is achieved. In (I.7) and (I.9), p_{T7} and p_{T0} correspond to interaction with environment and moving ground, respectively. Therefore, because of the fact that in our case, exoskeleton has a fixed base and no contact with environment, these terms vanished.

REFERENCES

- [1] Kazerooni, Hami, and S. L. Mahoney. "Dynamics and control of robotic systems worn by humans." (1991): 379-387.
- [2] Rebelo, Joao, et al. "Bilateral robot teleoperation: A wearable arm exoskeleton featuring an intuitive user interface." *IEEE Robotics & Automation Magazine* 21.4 (2014): 62-69.
- [3] Haddadin, Sami, and Elizabeth Croft. "Physical human-robot interaction." *Springer handbook of robotics*. Springer, Cham, 2016. 1835-1874.
- [4] Pervez, Aslam, and Jeha Ryu. "Safe physical human robot interaction-past, present and future." *Journal of Mechanical Science and Technology* 22.3 (2008): 469-483.
- [5] Zhang, Gao-Wei, et al. "Integrated observer-based fixed-time control with backstepping method for exoskeleton robot." *International Journal of Automation and Computing* 17.1 (2020): 71-82.
- [6] Brahmi, Brahim, et al. "Passive and active rehabilitation control of human upper-limb exoskeleton robot with dynamic uncertainties." *Robotica* 36.11 (2018): 1757-1779.
- [7] Brahim, Brahim, et al. "Iterative estimator-based nonlinear backstepping control of a robotic exoskeleton." *International Journal of Mechanical and Mechatronics Engineering* 10.8 (2016): 1375-1381.
- [8] Brahmi, Brahim, et al. "Adaptive tracking control of an exoskeleton robot with uncertain dynamics based on estimated time-delay control." *IEEE/ASME Transactions on Mechatronics* 23.2 (2018): 575-585.
- [9] Wu, Qingcong, Bai Chen, and Hongtao Wu. "Rbf-based adaptive backstepping sliding mode control of an upper-limb exoskeleton with dynamic uncertainties." *IEEE Access* 7 (2019): 134635-134646.
- [10] Brahmi, Brahim, et al. "Compliant control for wearable exoskeleton robot based on human inverse kinematics." *International Journal of Advanced Robotic Systems* 15.6 (2018): 1729881418812133.

- [11] Brahmi, Brahim, et al. "Adaptive force and position control based on quasi-time delay estimation of exoskeleton robot for rehabilitation." *IEEE Transactions on Control Systems Technology* 28.6 (2019): 2152-2163.
- [12] Yip, P. Patrick, and J. Karl Hedrick. "Adaptive dynamic surface control: a simplified algorithm for adaptive backstepping control of nonlinear systems." *International Journal of Control* 71.5 (1998): 959-979.
- [13] Zhou, Jing, Changyun Wen, and Ying Zhang. "Adaptive output control of nonlinear systems with uncertain dead-zone nonlinearity." *IEEE Transactions on Automatic Control* 51.3 (2006): 504-511.
- [14] Liu, Zhi, Fujie Wang, and Yun Zhang. "Adaptive visual tracking control for manipulator with actuator fuzzy dead-zone constraint and unmodeled dynamic." *IEEE Transactions on Systems, Man, and Cybernetics: Systems* 45.10 (2015): 1301-1312.
- [15] Li, Zhijun, et al. "Adaptive impedance control for an upper limb robotic exoskeleton using biological signals." *IEEE Transactions on Industrial Electronics* 64.2 (2016): 1664-1674.
- [16] He, Wei, Yuhao Chen, and Zhao Yin. "Adaptive neural network control of an uncertain robot with full-state constraints." *IEEE transactions on cybernetics* 46.3 (2015): 620-629.
- [17] Zhang, Gaowei, et al. "Iterative learning sliding mode control for output-constrained upper-limb exoskeleton with non-repetitive tasks." *Applied Mathematical Modelling* 97 (2021): 366-380.
- [18] Wu, Xiaoyu, et al. "Reference trajectory reshaping optimization and control of robotic exoskeletons for human-robot co-manipulation." *IEEE transactions on cybernetics* 50.8 (2019): 3740-3751.
- [19] Yu, Yajing, et al. "Neural adaptive distributed formation control of nonlinear multi-uavs with unmodeled dynamics." *IEEE Transactions on Neural Networks and Learning Systems* (2022).
- [20] Liu, Yusheng, and Xing-Yuan Li. "Decentralized robust adaptive control of nonlinear systems with unmodeled dynamics." *IEEE Transactions on Automatic control* 47.5 (2002): 848-856.
- [21] Haninger, Kevin, and Dragoljub Surdilovic. "Identification of human dynamics in user-led physical human robot environment interaction." 2018 27th IEEE International Symposium on Robot and Human Interactive Communication (RO-MAN). IEEE, 2018.
- [22] Malysz, Pawel, and Shahin Sirouspour. "A kinematic control framework for single-slave asymmetric teleoperation systems." *IEEE Transactions on Robotics* 27.5 (2011): 901-917.
- [23] Malysz, Pawel, and Shahin Sirouspour. "Nonlinear and filtered force/position mappings in bilateral teleoperation with application to enhanced stiffness discrimination." *IEEE Transactions on Robotics* 25.5 (2009): 1134-1149.
- [24] Lampinen, Santeri, et al. "Force-Sensor-Less Bilateral Teleoperation Control of Dissimilar Master-Slave System With Arbitrary Scaling." *IEEE Transactions on Control Systems Technology* 30.3 (2021): 1037-1051.
- [25] Abdossalami, Amin, and Shahin Sirouspour. "Adaptive control of haptic interaction with impedance and admittance type virtual environments." 2008 Symposium on Haptic Interfaces for Virtual Environment and Teleoperator Systems. IEEE, 2008.
- [26] Stroeve, Sybert. "Impedance characteristics of a neuromusculoskeletal model of the human arm I. Posture control." *Biological cybernetics* 81.5 (1999): 475-494.
- [27] Zhu, Wen-Hong. *Virtual decomposition control: toward hyper degrees of freedom robots*. Vol. 60. Springer Science & Business Media, 2010.
- [28] Mattila, Jouni, et al. "A survey on control of hydraulic robotic manipulators with projection to future trends." *iEeE/ASME Transactions on Mechatronics* 22.2 (2017): 669-680.
- [29] Koivumäki, Janne, and Jouni Mattila. "Stability-guaranteed force-sensorless contact force/motion control of heavy-duty hydraulic manipulators." *IEEE Transactions on Robotics* 31.4 (2015): 918-935.
- [30] Koivumäki, Janne, and Jouni Mattila. "Stability-guaranteed impedance control of hydraulic robotic manipulators." *IEEE/ASME Transactions on Mechatronics* 22.2 (2016): 601-612.
- [31] Zhu, Wen-Hong, and Septimiu E. Salcudean. "Stability guaranteed teleoperation: an adaptive motion/force control approach." *IEEE transactions on automatic control* 45.11 (2000): 1951-1969.
- [32] Luna, Cristobal Ochoa, et al. "Virtual decomposition control of an exoskeleton robot arm." *Robotica* 34.7 (2016): 1587-1609.
- [33] Hejrati, Mahdi and Jouni Mattila. "Decentralized Nonlinear Control of Redundant Upper Limb Exoskeleton with Natural Adaptation Law." *arXiv preprint arXiv:2208.12184v1* (2022), accepted.
- [34] Chen, Mou, Shuzhi Sam Ge, and Bernard Voon Ee How. "Robust adaptive neural network control for a class of uncertain MIMO nonlinear systems with input nonlinearities." *IEEE Transactions on Neural Networks* 21.5 (2010): 796-812.
- [35] Tee, Keng Peng, Shuzhi Sam Ge, and Eng Hock Tay. "Barrier Lyapunov functions for the control of output-constrained nonlinear systems." *Automatica* 45.4 (2009): 918-927.
- [36] Lee, Taeyoon, Jaewoon Kwon, and Frank C. Park. "A natural adaptive control law for robot manipulators." 2018 IEEE/RSJ International Conference on Intelligent Robots and Systems (IROS). IEEE, 2018.
- [37] Liñán, Ma del Carmen Rodríguez, and William P. Heath. "Controller structure for plants with combined saturation and deadzone/backlash." 2012 IEEE International Conference on Control Applications. IEEE, 2012.



Mahdi Hejrati received his M.Sc. degree in 2021 from Sharif University of Technology (SUT), Tehran, Iran. He is currently a PhD student at the unit of Automation Technology and Mechanical Engineering, Tampere University, Tampere, Finland. His research interests include nonlinear model-based control and Intelligent control.



Jouni Mattila Dr. Tech. received his M.Sc. (Eng.) in 1995 and Dr. Tech. in 2000, both from Tampere University of Technology (TUT), Tampere, Finland. He is currently a Professor of machine automation with the unit of Automation Technology and Mechanical Engineering, Tampere University. His research interests include machine automation, nonlinear model-based control of robotic manipulators and energy-efficient control of heavy-duty mobile manipulators.